J Mater Sci (2007) 42:30–39
DOI 10.1007/s10853-006-1039-y

Fabrication and characterization of vacuum plasma sprayed W/Cu-composites for extreme thermal conditions

G. Pintsuk · I. Smid · J.-E. Döring · W. Hohenauer · J. Linke

Received: 20 September 2005 / Accepted: 18 January 2006 / Published online: 14 November 2006

Abstract The joining of tungsten to copper and the ongoing search for commercially viable production techniques is one of the challenging issues in the field of composite materials. The reason why this material combination is of essential importance is its ability to withstand erosion and high temperatures on the tungsten side and to remove big quantities of heat on the copper side. Due to the mismatch of thermal expansion and Young's moduli, the direct joining of these two materials results in high residual and thermal stresses at the interface, ultimately reducing component lifetime. One potential answer to this problem is functionally graded structures of W and Cu, which smoothen the transition of material properties. The present study focuses on vacuum plasma spraying (120 mbar, Ar) of W/Cu-gradients and composites with defined mixing ratios. The influence of the fabrication process and the W:Cu ratio on the microstructure has been investigated and results from thermo-mechanical and thermo-physical results analyses are presented. Finite element modeling has been used to demonstrate the positive effect of gradients on the elastic and elastic–plastic response within two different model-geometries. Partial gradients, ranging from pure tungsten to 75 vol.% tungsten, exhibit the best results and improve the expected life-time performance significantly by reducing the stresses at both interfaces, W/FGM and FGM/Cu, compared to a reference interface between W and Cu.

G. Pintsuk (✉) · J.-E. Döring · J. Linke
Forschungszentrum Jülich, Euratom-Association,
D-52425 Julich, Germany
e-mail: g.pintsuk@fz-juelich.de

I. Smid
The Pennsylvania State University, University Park
PA 16802, USA

W. Hohenauer
ARC Seibersdorf Research GmbH, A-2444 Seibersdorf,
Austria

Introduction

The field of possible applications of W/Cu-composites varies over a wide range, which includes components in military, space and nuclear fusion technologies as well as parts in electronic devices (heat sinks) and energy systems (e.g., contact material in power switches) [1, 5]. In every case it is used to deal with thermal and often extreme thermal conditions.

The choice of joining techniques for tungsten and copper is strongly connected to big differences in melting temperatures and densities. Various methods of forming combinations of these materials either with fixed compositions or as graded structures have been investigated [6–19]. The motivation to determine new ways of designing gradients is in their ability to reduce thermal stresses [20–23]. At the W/Cu-interface, huge differences in Young's moduli ($\Delta E \approx 300$ GPa) and thermal expansion coefficients ($\Delta\alpha \approx 12 \times 10^{-6}$ K^{-1}) occur, which is critical for lifetime. By smoothing the transition of properties at the interface of W/Cu-laminates via a functionally graded material (FGM), an increase in the lifetime of thermally loaded structural parts can be obtained.

This paper focuses on vacuum plasma spraying (VPS) and the evaluation of microstructural, mechanical,

and thermo-physical properties of W/Cu-composites with a defined mixing ratio. By inserting this data into elastic and elasto-plastic finite element analyses, further optimizations of the graded structure can be achieved.

Vacuum plasma spraying—experimental

The W/Cu-coatings were deposited by VPS in a plasma-spray facility manufactured by Sulzer-Metco, Wohlen, Switzerland. In the VPS process the powder particles of the material to be deposited on a given substrate are blown into a plasma plume produced by a certain gas mixture in an ambient Ar-atmosphere of 120 mbar. Therein they are melted, accelerated towards the substrate and finally each particle is deposited on the substrate in a splat like structure using mechanical bonding. The current was 740 A, which results in 50 kW power output, the plasma gas flow was 40/10 SLPM (standard liters per minute) Ar/H_2 and the feeding gas flow amounted 1 SLPM argon gas in the case of copper and 0.7 SLPM in the case of tungsten [12].

The parameters have been optimized for W-particles with an average diameter of 5.5 μm (Fig. 1a), provided by Plansee AG (Reutte, Austria). The Cu-powder, provided by MicroMet with a particle size <100 μm (Fig. 1b), has been adjusted to the evaluated W-parameters and therefore sieved to a fraction of 40–50 μm. The powders were mixed in the plasma plume by using two separate powder feeding systems: injecting tungsten from top, copper from beneath. The feed rates, which are linearly dependent on the rotation speed, have been evaluated at 4 rpm and amount to 2.66 g/min for Cu and 10.84 g/min for W. By individually changing the rotation speed either of the W or the Cu powder feeder any desired composition can be produced. The different behavior of the particles in the plasma plume is highlighted in Fig. 2. Forming a narrow beam, W is leaving the plume in an angular range of 1–5° below the axis set up by the spraying direction. In contrast, Cu is ejected in a broad angular field mainly above this axis.

Additionally, transferred arc-cleaning (TAC) has been used during all experiments for in situ purification of the layer surface by the removal of loose particles [12, 24]. TAC is used for the removal of loose material, which leads to a densification of the material and an improved connectivity of the single phases.

Metallography

Four W/Cu-coatings (Fig. 3) with a thickness of 2–3 mm and a Cu-content of (a) 26, (b) 43, (c) 52, and (d) 78 vol.%, measured by image analysis (KS 400 3.0, Zeiss) of the polished cross-section, have been deposited on graphite substrates (area = 50 mm × 50 mm). Graphite substrates have been used to ease the removal of the coating and to obtain free standing layers.

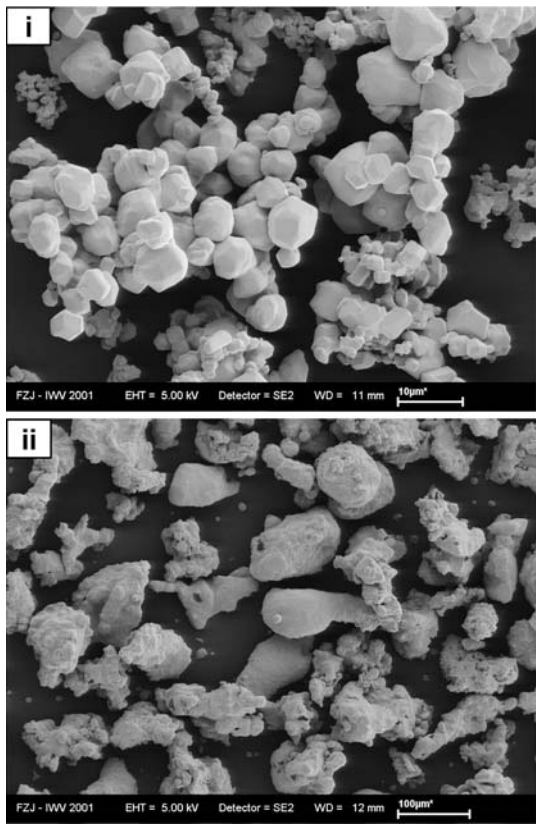

Fig. 1 SEM-pictures of (**i**) W-powder, 1–10 μm, Plansee AG and (**ii**) Cu-powder, <100 μm, MicroMet

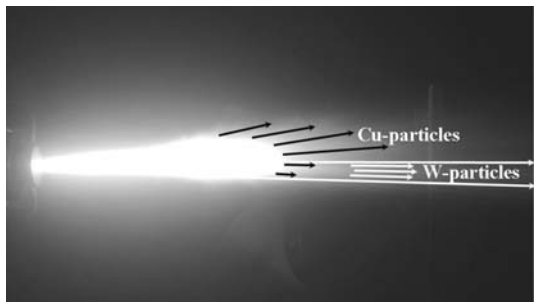

Fig. 2 W/Cu in the plasma plume—broad emission of Cu, narrow emission of W

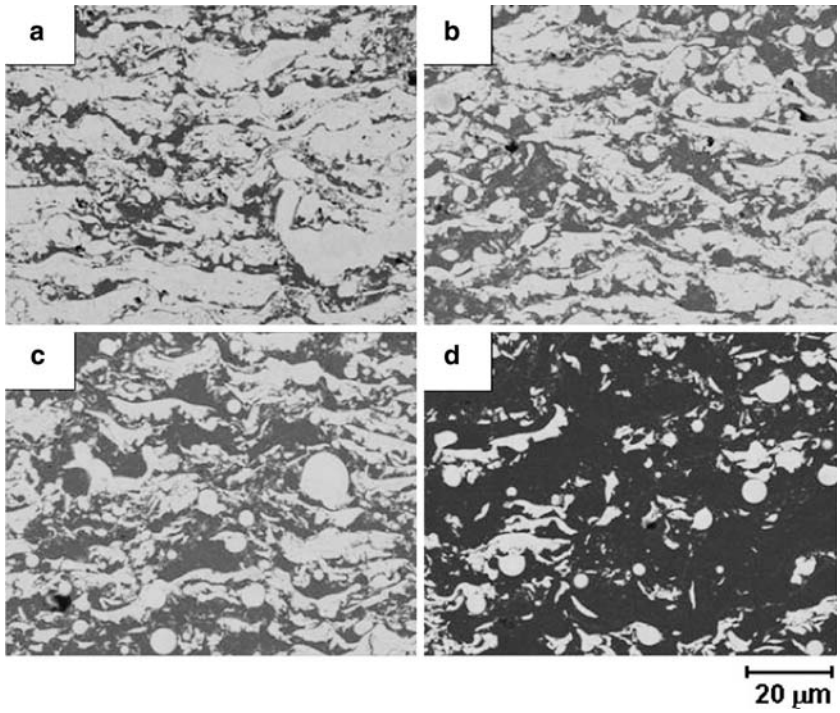

Fig. 3 SEM pictures of VPS-samples with different volume fractions of W and Cu. Use of two seperate powder feeding systems—content of unmolten particles, porosity by image analysis <1%; (**a**) 26 vol.% Cu, (**b**) 43 vol.% Cu; (**c**) 52 vol.% Cu; (**d**) 78 vol.% Cu

All four compositional microstructures are characterized in terms of embedded molten and unmolten W-particles. The volume fraction of spherical, unmolten particles has been determined by optical analysis and amounts to ~6%. It is independent from the total W-content in the composite and the particle size varies over the whole dimensional range from 2 to 9 µm. Hence the size is not the critical parameter to melt the particles. The key parameter influencing the status of melting is the trajectory of the particles. Nevertheless, the distribution of those particles from the microstructural point of view is quite uniform, although a macroscopically measurable decrease in mechanical strength is assumed. In contrast, the distribution of the entirely molten Cu-phase within the material is regarded as homogeneous, which results in a connected Cu-structure throughout the material similar to infiltrated W/Cu-composites and hence thermal conductivities are improved to reasonably high values. This is due to variations in particle behavior within the plasma plume, mentioned above, and verified by investigations of the microstructure of the fracture surface of W-74 vol.% Cu at RT and 600 °C, obtained after four-point-bending. At room temperature (RT), the fracture surface is dominated by brittle cracking of W (Fig. 4a), whereas Cu reveals a honeycomb structure characteristic for ductile materials. At 600 °C, the crack runs all through the Cu-phase, including small islands of W (Fig. 4b).

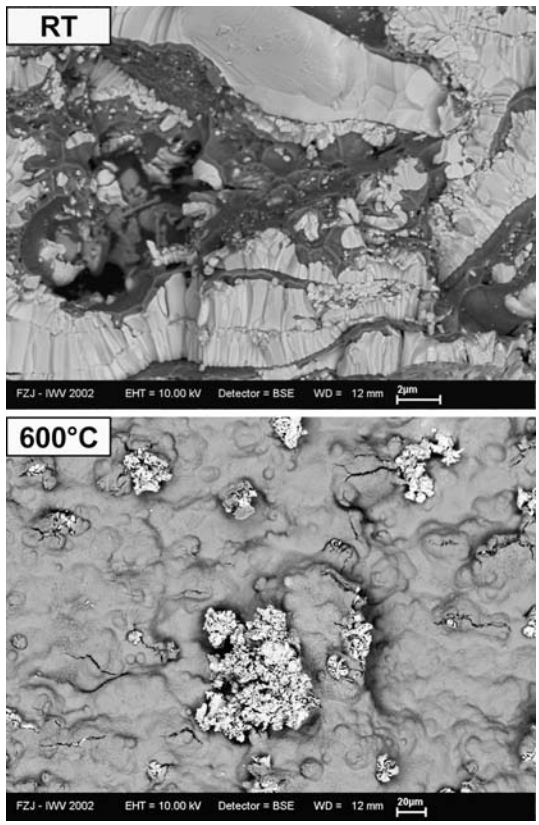

Fig. 4 SEM-pictures of fracture surfaces of W–74 vol.% Cu after four-point-bending at RT and 600 °C

Due to the use of a low pressure Ar-atmosphere of 120 mbar during operation and TAC as auxiliary means oxidation can be strongly reduced and optimized thermo-physical properties obtained. In EDX-line profiles, shown in Fig. 5, oxygen has been detected between the phases whereby the objective of a maximum in bonding strength and transfer of thermal energy is achieved.

Furthermore parts of each produced layer have undergone a heat treatment at 1,050 °C (1 h, hydrogen atmosphere). The measurement of density by optical analysis before and after revealed significant changes, depending on the Cu-content in the structure. The density (Table 1) increases as a result of the heat treatment which is correlated to initial density values after production and therefore exhibits the highest results for sample (a).

With regard to the co-action of deposition rate, which is in the range of 5–8 µm/cycle, and powder feed rate for each material to obtain defined mixing ratios, two graded structures have been fabricated. One is a functionally graded structure with a total thickness of 1.1 mm having a ''full gradient'' in the range from pure tungsten to pure copper, the other one is a 2.5 mm thick ''partial gradient'', running from 95 to 75 vol.% W and having a bonding layer with approximately 20 vol.% W-content for the integration into components. Both microstructures in Fig. 6 exhibit homogeneous phase distributions and smooth transitions between different compositions (Fig. 7). As mentioned before, a porosity increase up to 10% (measured by optical means, image analysis) is related to a decrease in Cu-content.

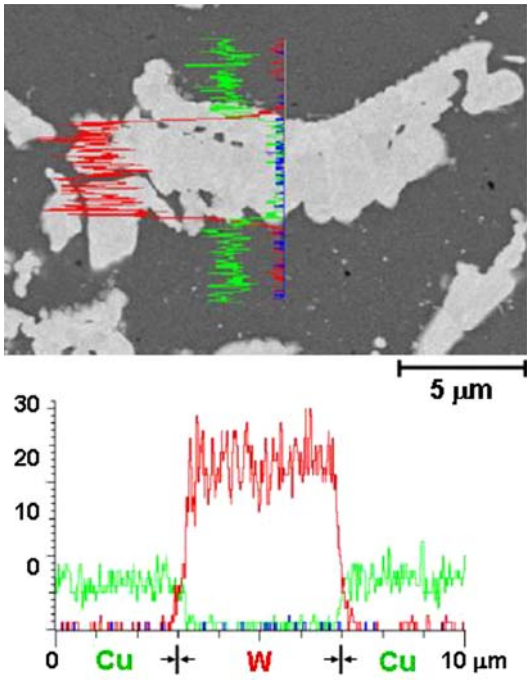

Fig. 5 EDX-line scan of VPS-coatings to evaluate possible oxide formation at the interfaces between W and Cu: no oxide detected

Material testing and characterization

Mechanical testing: static

Four-point-bending tests at RT, 200, 300, and 600 °C have been performed on samples with an area of 50 mm × 4 mm and a thickness of 2–3 mm. The cutting of the samples has been done by wire-erosion. Stress–strain curves of the different W/Cu-compounds, the yield strength $R_{p,0.2}$ (Table 2) and their Young's moduli in dependence on the temperature have been evaluated, see Fig. 8. Although neither the elastic modulus of 400 GPa for pure W, nor 120 GPa for pure Cu have been achieved by the plasma sprayed material, these values are, compared to other production methods, rather good and a proof of quality [3].

The Young's modulus, a measure of the stiffness, remains constant up to 300 °C, observed for all compositions with 43 vol.% Cu or higher. A consequence of this is the existence of a strengthening mechanism, with a dependence on the Cu-content, the thermo-mechanical behavior of Cu and the porosity within the composite. Filling of gaps, which have been formed during cool-down and have not become evident in microstructural analyses due to smearing of copper, and in relation to this the formation of compressive stresses within the material are assumed to be the main reasons. A limitation to this strengthening effect is set by the softening of Cu and the resulting significant increase in ductile deformation with increasing temperature, caused by a temperature dependent reduction in yield strength. Therefore, with increasing temperature and Cu-content, a reduction in stiffness is observed (Fig. 8).

Table 1 Density before and after heat treatment (1,050 °C, 1 h, hydrogen atmosphere) of plasma-sprayed layers

No.	Composition (vol.%)	ρ (g/cm^3)		Difference, $\Delta\rho$ (g/cm^3)
		Before heat treatment	After heat treatment	
a	W–26Cu	15.16	15.67	0.51
b	W–43Cu	14.04	14.43	0.39
c	W–52Cu	12.48	12.74	0.26
d	W–78Cu	10.50	10.68	0.18

Fig. 6 LM-pictures of graded structures sprayed by VPS with different compositions: (**i**) full gradient from pure W to pure Cu, (**ii**) partial gradient from pure W to a maximum Cu-content of 25 vol.% with an 80 vol.% Cu bonding layer of 50 μm (Fig. 7)

At a temperature of 600 °C, another effect becomes apparent comparing samples (b) and (c) (see Fig. 3). Within this range a loss of more than 30% of stiffness (and strength, too) is measured, reflecting the transition in microstructure from a stabilizing W-skeleton to a Cu-skeleton.

Mechanical testing: dynamic

Dynamic material properties were calculated via measuring of longitudinal and transversal sound velocity c_L and c_T at a frequency of 10 MHz in an ultrasonic test facility of the type Panametrics Multiscan. The shear modulus G_{dyn} was determined by

$$G_{dyn} = c_T^2 \rho \tag{1}$$

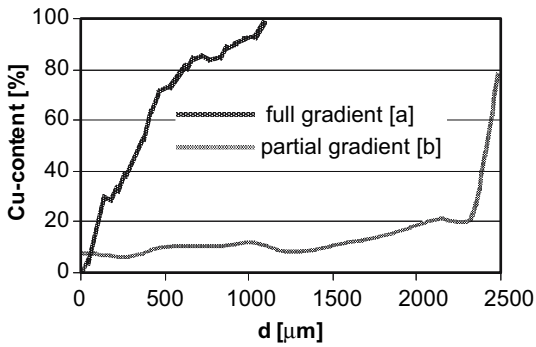

Fig. 7 Composition curves for graded composites (Fig. 6)

Table 2 Yield strength $R_{p,0.2}$ from RT to 600 °C for different material compositions

No.	Composition (vol.%)	$R_{p,0.2}$ [MPa]			
		RT	200 °C	300 °C	600 °C
a	W–26Cu	445	424	404	224
b	W–43Cu	335	351	340	179
c	W–52Cu	276	284	271	127
d	W–78Cu	202	208	182	72

and the dynamic Young's modulus E_{dyn} by taking the Poisson's ratio ν into account

$$E_{dyn} = c_L^2 \rho \frac{(1+\nu)(1-2\nu)}{(1-\nu)}$$
$$\nu = \frac{1-2(c_T/c_L)^2}{2-2(c_T/c_L)^2} \tag{2}$$

In the dynamic analyses, where ρ is the composite density, comparable values to static Young's moduli have been determined for W-78Cu and W-52Cu (Fig. 9). Due to the distortion of the acoustic signal caused by an increase in porosity with increasing

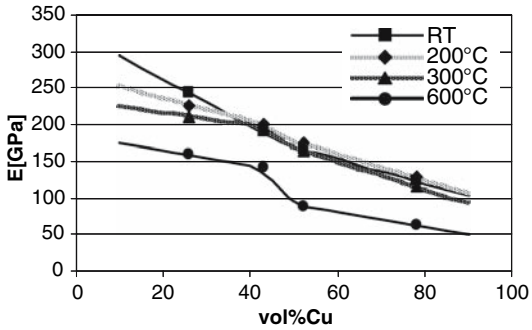

Fig. 8 Temperature dependent values of Young's modulus for various W/Cu-composites manufactured by VPS

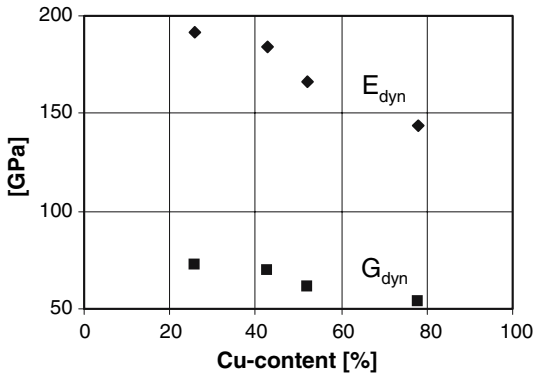

Fig. 9 Dynamic measurement of properties of plasma-sprayed W/Cu-composites. Young's modulus and shear modulus

tungsten content lower values have been found for W-43Cu and W-26Cu. For both, dynamic shear and Young's moduli (Fig. 9), a change in material behavior becomes apparent, which is related to the content of Cu and W, respectively.

Dilatometry

The coefficients of thermal expansion (CTE) have been evaluated for all W/Cu-composites before and after the heat treatment at 1,050 °C in hydrogen (Fig. 10). At higher Cu contents in materials before heat treatment, the CTE decreases between 500 and 700 °C. In general, those curves are typical for bimetals and also very soft materials and are related to bending and elasto-plastic deformation. A maximum drop in CTE of ~21% or ~3×10^{-6} K^{-1} is obtained for composition (78 vol.% Cu), which occurs in the range between 1,000 and 1,050 °C, close to the melting point of Cu (1,083 °C). Sintering effects might have a significant effect, too, because this tendency is reversed after sintering. In general an increase in CTE is observed after the heat treatment. This means for sample (c, 52 vol.% Cu) at 200 °C a rise in CTE of 1.2×10^{-6} K^{-1} and for sample (d, 78 vol.% Cu) a rise of 0.4×10^{-6} K^{-1}. At 800 °C measurements yield differences of 1.5×10^{-6} K^{-1} for (c) and 0.8×10^{-6} K^{-1} for (d). W/Cu-composites with a microstructure dominated by a tungsten skeleton exhibit no change in their behavior and CTE values.

Testing of FGMs (Fig. 11), which have been produced with and without transferred arc cleaning (TAC) revealed significant differences. Without TAC, bending of the sample already started at 300 °C, whereas the sample with TAC retained its strength until a temperature of 950 °C, which enhances the quality of the material significantly.

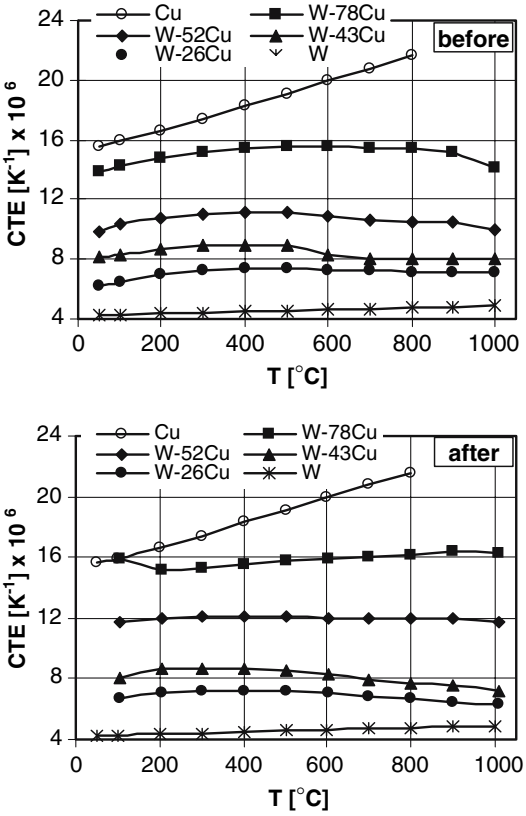

Fig. 10 CTE of VPS-W/Cu-coatings before and after heat treatment at 1,050 °C in H_2-atmosphere

Thermal conductivity

Considering that thermal conductivity is a product of density (Table 1), thermal diffusivity and specific heat (Fig. 12), laser-flash measurements have been carried out in two different testing facilities to confirm the evaluated data. Low values at RT, which are less important for high temperature applications of W/Cu-materials, and maxima, which are shifted to higher temperatures when increasing the Cu-content, are the most important characteristics of the determined thermal diffusivities.

The measured specific heat at RT is in very good agreement with calculations using the rule of mixture

$$\begin{aligned} c_{W/Cu} &= \frac{1}{\rho_{W/Cu}}\left(k_W \rho_W c_W + k_{Cu}\rho_{Cu}c_{Cu}\right) \\ k_W &= 1 - k_{Cu} \end{aligned} \quad . \tag{3}$$

where k is the volume fraction, ρ the density and c the specific heat of the particular material. Since the measured specific heat increases just slightly or remains constant with increasing temperature, the

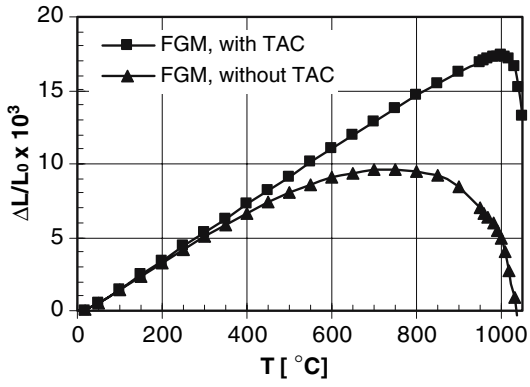

Fig. 11 Thermal strain measurement of plasma sprayed graded W/Cu-composites with a full gradient from pure W to pure Cu. Fabrication with and without transferred arc cleaning (TAC). Bending during testing

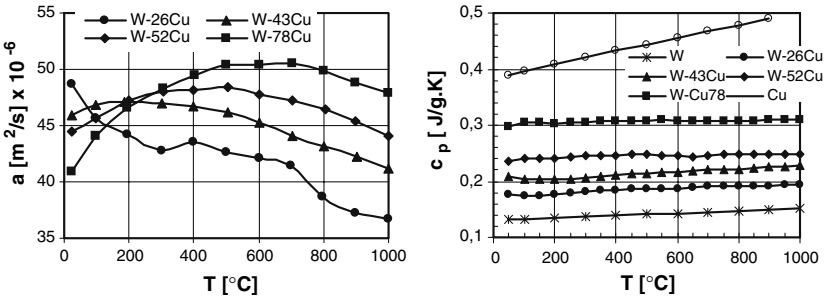

Fig. 12 Thermal diffusivity (left) and specific heat (right) of VPS-W/Cu-coatings

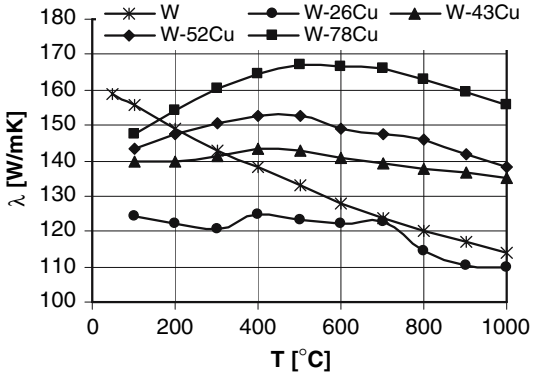

Fig. 13 Thermal conductivity of VPS-W/Cu-coating

thermal conductivity functions (Fig. 13) exhibit the same characteristics as mentioned for thermal diffusivity. The calculated data points at RT are located within the range of pure tungsten (161 W m^{-1} K^{-1}) and a long way off the value for pure copper (398 W m^{-1} K^{-1}). The reasons for these low values are on the one hand the existing porosity and on other hand a certain lack in connectivity among the phases, caused by contraction during cool-down after deposition. By an increase in temperature and the related expansion of the materials the formed gaps are closed again. At 600 °C the medium values of the thermal conductivity are (a, 26 vol.% Cu) 167 W m^{-1} K^{-1} (b, 43 vol.% Cu) 149 W m^{-1} K^{-1} (c, 52 vol.% Cu) 141 W m^{-1} K^{-1}, and (d, 78 vol.% Cu) 122 W m^{-1} K^{-1}, and are situated in the intermediate range between W and Cu, comparable to extrapolated results of Itoh et al. on VPS [25], but are still below those of comparable infiltrated W/Cu-composites [3].

Finite element modeling

The finite element code ANSYS was used to predict the ability of graded plasma sprayed W/Cu materials to reduce the stresses at the joint between W and Cu. Therefore, two cross-sections of a cylinder with diameters of 5 and 20 mm, respectively, were analyzed (Fig. 14). For both, a reference model without FGM (the FGM portion is replaced by W) and two models containing FGMs were compared (Table 3). The FGM

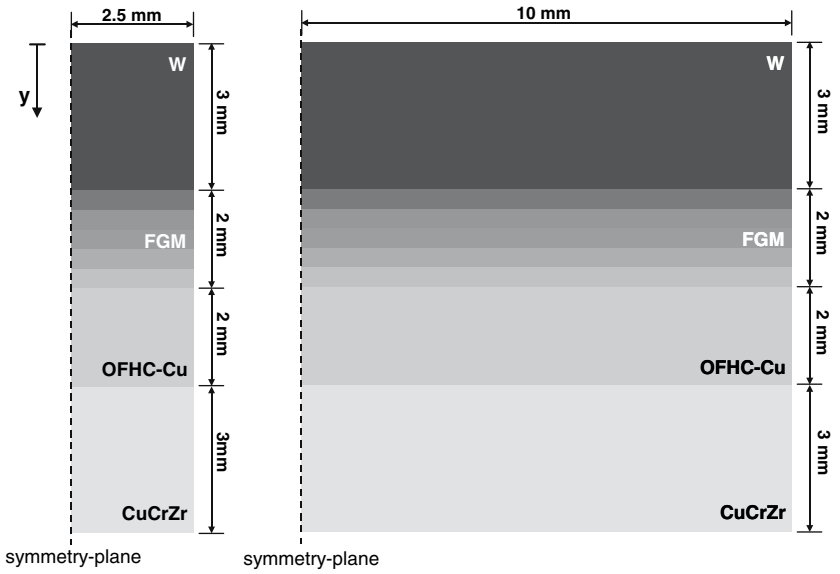

Fig. 14 Cross-sections of two cylindrical probes (∅ = 5 and 20 mm) with integrated W/Cu-gradient. Symmetry used for computational analysis

Table 3 Composition and thickness of the individual sub-layers within the model of a continuous and a partial gradient system (Figs. 6 and 7)

Composition (vol.% W)	Thickness (mm)
Continuous FGM	
10	0.4
30	0.4
50	0.4
70	0.4
90	0.4
Total	2
Partial FGM	
75	0.4
80	0.4
85	0.4
90	0.4
95	0.4
Total	2

was modeled as five-layer system with a defined layer thickness and a variation in composition. The material input data and there most important the plasticity behavior (Table 4) has been determined from the above measured material properties for certain compositions by extrapolation over the whole compositional range. A simplification of both models was achieved by taking symmetry into account and by the assumption of perfect bonding at the material joints. As a boundary condition, the stress free temperature was set to 500 °C, which corresponds to the advised fabrication temperature during the HIP-process.

In the simulation, quadrilateral four-node elements (PLANE42) with an element size of ~0.06 mm^2 were used for the structural analyses. Elastic and elastic–plastic residual stresses at RT were calculated and the x-directional stresses in the symmetry axis (Fig. 14) extracted, starting from the W-surface ($y = 0$; Figs. 15–18). The comparison of stresses was done at the symmetry axis since the interpretation of stresses at the outer surface is very difficult due to occurring

Table 4 Extrapolated temperature dependent mechanical properties of plasma sprayed W/Cu-composites with selected compositions as input data for elastic–plastic analyses

Composition (vol.%)	T (°C)	E (GPa)	YS (MPa)	UTS (MPa)
W–20Cu	20	262	481	985
	200	236	450	900
	600	166	240	470
W–40Cu	20	198	363	710
	200	204	364	664
	600	146	187	300
W–60Cu	20	154	253	467
	200	160	261	436
	600	81	110	180

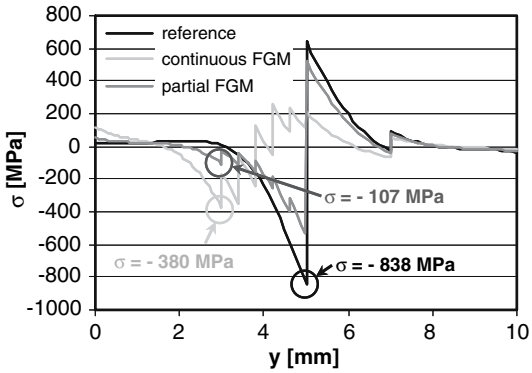

Fig. 15 Elastic stresses σ_x in the symmetry plane of the cylindrical geometry with 5 mm in diameter, starting from the W surface (0 mm, Fig. 14)

singularities, characterized by an element size dependent stress increase.

Elastic analysis

The two most important results in this qualitative analysis are: (1) occurrence of a size effect as an influencing factor on the stress level; (2) the ability of FGMs to reduce thermal induced stresses. The first point is related to a decrease in stress within the whole component in relation to a reduction in diameter. This effect is independent of the existence or non-existence of an FGM. Especially at the outer surfaces ($d = 0$ and 10, Figs. 15 and 16) the difference is outlined by almost disappearing stresses for small diameters in contrast to high tensile stresses in W, and compressive stresses in CuCrZr, which are characteristic for the large model geometry.

Dealing with the ability of F7GMs to reduce thermal stresses (point 2) it becomes evident that for both reference models without FGM high compressive

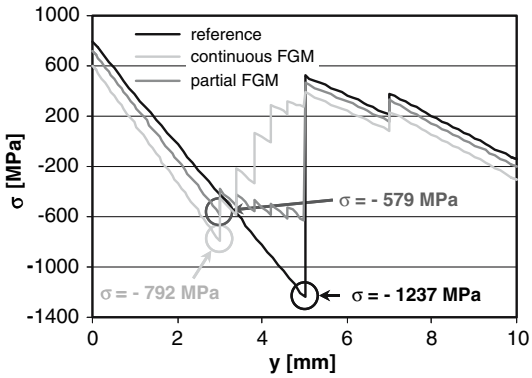

Fig. 16 Elastic stresses σ_x in the symmetry plane of the cylindrical geometry with 20 mm in diameter, starting from the W surface (0 mm, Fig. 14)

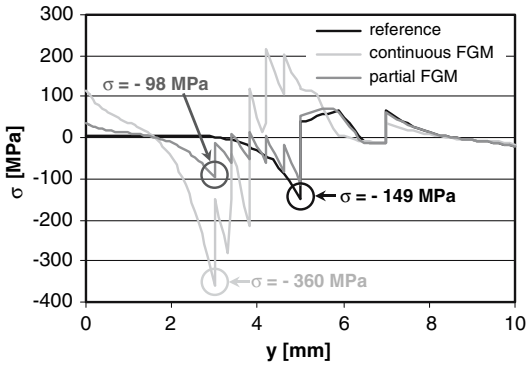

Fig. 17 Elasto-plastic stresses σ_x in the symmetry plane of the cylindrical geometry with 5 mm in diameter, starting from the W surface (0 mm, Fig. 14)

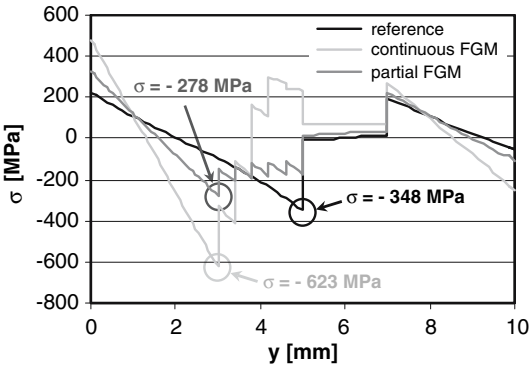

Fig. 18 Elasto-plastic stresses σ_x in the symmetry plane of the cylindrical geometry with 20 mm in diameter, starting from the W surface (0 mm, Fig. 14)

stresses in W and high tensile stresses in Cu arise at the W/OFHC-Cu interface (Figs. 15 and 16), apparently the most crucial part in the structure. Further, the reference stresses in W are considered as representative for the overall model behavior. By introducing an FGM between W and OFHC-Cu these stresses are, now at the W/FGM-interface and irrespective of the component size, reduced by a continuous gradient by 55% (∅ = 5 mm) and 36% (∅ = 20 mm) and by a partial gradient by 87% (∅ = 5 mm), and 53% (∅ = 20 mm). This shows that a reduction depends on the composition of the graded interface and is significantly enhanced by the use of a partial gradient with a high W-content.

The stress evolution within the gradients is strongly influenced by the compositional differences. For the partial gradient, the stresses within the FGM and at the FGM/OFHC-Cu interface continue to be compressive and are increased to $\sigma_{FGM/Cu}$ = –527 MPa (∅ = 5 mm, Fig. 15) and $\sigma_{FGM/Cu}$ = –627 MPa (∅ = 20 mm, Fig. 16), but are still below the maximum values of the reference model without FGM. In contrast, with increasing Cu content in the gradient layer a transition from compressive to tensile stresses occurs leading to tensile stresses at the FGM–OFHC–Cu joint of $\sigma_{FGM/Cu}$ = 113 MPa (∅ = 5 mm, Fig. 15) and $\sigma_{FGM/Cu}$ = 269 MPa (∅ = 20 mm, Fig. 16). Additionally, the stresses in the OFHC-Cu interlayer are, especially for the smaller diameter (Fig. 15), strongly reduced by the continuous gradient.

Elastic–plastic analysis

When taking into account plastic deformation, one unexpected result becomes apparent: using a continuous gradient deteriorates rather than improves the stress state in the composite structure (Figs. 17 and 18). Moreover, comparing elastic and elastic–plastic computational results, the stresses caused by the continuous gradient basically remain almost constant. In

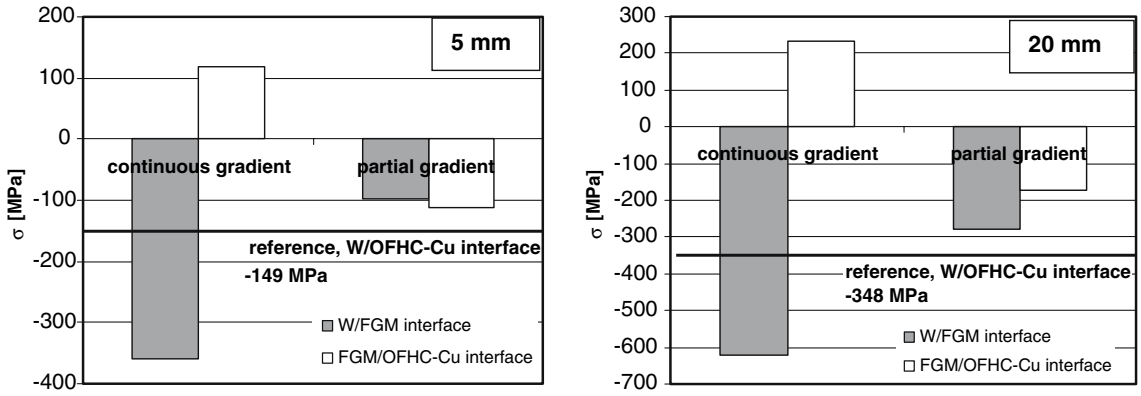

Fig. 19 Maximum elasto-plastic stresses σ_x at the interfaces between W and FGM and between FGM and OFHC-Cu for 5 and 20 mm cylinder diameter. Comparison of the reference stresses at the interface between W and OFHC-Cu and the continuous and partial FGM (Table 3)

contrast, this comparison shows that the reference and the component with the partial gradient are characterized by a strong reduction in (i) compressive stresses at the W/OFHC-Cu (up to ~82%) and FGM/OFHC-Cu (up to ~79%) interface, respectively, and (ii) tensile stresses (>90%) at the same joints.

In conclusion, it can be stated that only a partial FGM, containing a high W-content, is able to improve and to reduce the life-limiting stresses significantly, while a continuous gradient would increase compressive and even generate tensile stresses (Fig. 19). These results are valid for both investigated cylindrical geometries with diameters of 5 and 20 mm. The reason for this behavior is that because of the high stiffness and yield strength of the plasma sprayed material, compared to pure Cu, the same strain results in higher stresses. Since also the CTE increases significantly with increasing Cu-content (especially from 40 to 60 vol.% Cu due to microstructural changes, see above) high thermal strains and therefore stresses are formed in the FGM. This is related to the interaction of tungsten and the FGM, which can only be avoided by keeping the CTE and therefore the strain within the FGM as low as possible. Furthermore, the stresses are also affected by component size, yielding more than 50% lower stresses for the smaller diameter compared to the larger one.

Conclusion

Vacuum plasma spraying was found to be a very good method to produce graded W/Cu-composites which exhibit homogeneous distributions of W and Cu in the composite, no oxidation, sufficiently high density and good thermal conductivity, especially at higher temperatures. Variations within the whole composition range are possible and, due to a low deposition rate during plasma spraying of 6–10 μm per cycle, every desired gradient function and continuous gradients are achieved.

From elastic and elastic-plastic FEM-analyses, partial gradients from 75 vol.% to pure W and small component geometries ($\varnothing \leq 5$ mm) are able to minimize the thermally induced stresses in a W/Cu-component. For a given cylindrical geometry with a diameter of 5 mm, the life limiting stresses at the interface are reduced by ~35% which will extend the expected life-time performance significantly.

Acknowledgements The supply of W-powders by the Plansee AG and funding by the Austrian ''Friedrich Schiedelstiftung für Energietechnik'', which made this project possible, are gratefully acknowledged.

References

1. Brookes KJA (2000) PM Technology Trends, pp 16–18
2. Joensson M, Kieback B (2001) 15th Int Plansee Seminar, vol 1, RM 3, pp 1–15
3. Itoh Y, Takahashi M, Hirohisa H (1996) Fus Eng Des 31:279
4. Hino T, Akiba M (2000) Fus Eng Des 49–50: 97
5. Ge CC, Zhou ZJ (2005) Mater Sci For 475–479: 1371
6. Kieback B, Neubrand A, Riedel H (2003) Mater Sci Eng A 362: 81
7. Birth U, Joensson M, Kieback B (1999) Mater Sci For 308–311: 766
8. Ge CC, Li JT, Zhou Z-J, Cao W-B, Shen W-P, Wang M-X, Zhang N-M, Liu X, Xu Z-Y (2000) J Nucl Mater 283–287: 1116
9. Pintsuk G, Brünings SE, Döring J-E, Linke J, Smid I, Xue L (2003) Fus Eng Des 66–68: 259
10. Gomes UU, da Costa FA, da Silva AGP (2001) 15th Int Plansee Seminar, vol 1, RM 24, pp 177–189
11. Jedamzik R, Neubrand A, Rödel J (2000) J Mater Sci 35:477
12. Döring JE, Vaßen R, Pintsuk G, Stöver D (2003) Fus Eng Des 66–68: 259
13. Wang S-H, Xue L (2005) Surf Eng Mater Sci III: 27
14. Pintsuk G, Hohenauer W, Linke J, Smid I, Wang S-H, Xue L (2005) 16th Int Plansee Seminar, vol 1, PL11, pp 131–143
15. Johnson J, German R (2005) 16th Int. Plansee Seminar, vol 1, PL10, pp 116–130
16. Sabirov I, Pippan R (2005) 16th Int. Plansee Seminar, vol 1, RM28, pp 291–299
17. Shen W-P, Zhou Z-J, Gu S-Y, Ge C-C, Zhang H, Liu H-L (2005) Mater Sci For 475–479: 1563
18. Xie J-X, Li S-B, Chen S (2005) Mater Sci For 475–479: 1511
19. Kang H-K (2004) Scr Mater 51:473
20. Hamatani H, Shimoda N, Kitaguchi S (2003) Sci Tech Adv Mater 4:197
21. Shabana YM, Noda N (2001) Comp Part B 32:111
22. Gasik MM (1998) Comp Mater Sci 13:42
23. Chapa J, Reimanis I (2002) J Nucl Mater 303:131
24. Hollis KJ, Castro RG, Doerner RP, Maggiore CJ (2001) Fus Eng Des 55:437
25. Itoh Y, Andoh H, Suyama S, Shindoh T (2001) J Jpn Inst Met 65(12):1108